ACS Catalysis

pubs.acs.org/acscatalysis Research Article

Substrate Tunnel Engineering Aided by X-ray Crystallography and Functional Dynamics Swaps the Function of MIO-Enzymes

Zsófia Bata, Zsófia Molnár, Erzsébet Madaras, Bence Molnár, Evelin Sánta-Bell, Andrea Varga, Ibolya Leveles, Renzhe Qian, Friedrich Hammerschmidt, Csaba Paizs,* Beáta G. Vértessy,* and László Poppe*

Cite This: https://doi.org/10.1021/acscatal.1c00266 Read Online

ACCESS | Metrics & More | Article Recommendations | Supporting Information

ABSTRACT: The enzyme family harboring the post-translationally formed 5-methylene-3,5-dihydro-4*H*-imidazol-4-one (MIO) catalytic residue comprises both aromatic amino acid ammonia-lyases (ALs) and 2,3-aminomutases (AMs). The structural origin of the different functions and the role of the inner loop region in substrate binding are not fully understood. Here, we provide the three-dimensional structures for *Petroselinum crispum* phenylalanine AL (PcPAL) with fully resolved inner loops in a catalytically competent conformation. Using molecular modeling, we demonstrate that in both ALs and AMs of eukaryotic origin, just a small opening of the inner loop is sufficient for ligand egress. Furthermore, we show that ligand-binding tunnels are analogous to eukaryotic MIO-enzymes and that the critical initial part of these tunnels is present across the whole enzyme family. Engineering of these binding tunnels converts an (*R*)-AM to a highly selective (*S*)-β-AL thus establishing a nonclassified enzyme function.

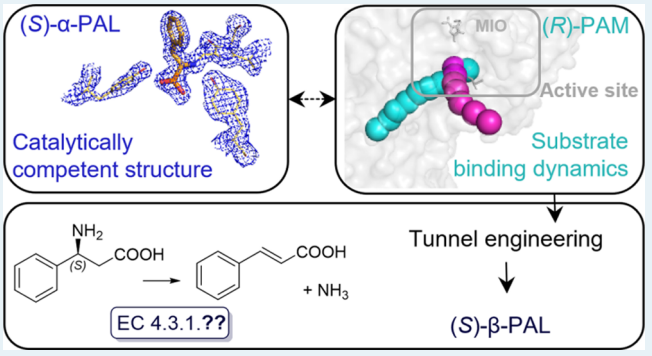

KEYWORDS: *biocatalysis, class I lyase-like enzyme, phenylalanine ammonia-lyase, phenylalanine 2,3-aminomutase, crystal structure, mechanism-based inhibition, substrate-binding dynamics, tunnel engineering*

INTRODUCTION

The 5-methylene-3,5-dihydro-4*H*-imidazol-4-one (MIO)-containing class I lyase-like enzyme family (MIO-enzymes) constitutes two functionally diverse but structurally related enzyme classes, the aromatic amino acid ammonia-lyases (ALs) and the aromatic amino acid 2,3-aminomutases (AMs).[1] ALs catalyze the reversible ammonia elimination from histidine, phenylalanine, or tyrosine (HALs, PALs, and TALs, respectively; Figure 1a), using a special post-translationally formed residue, MIO, as the catalytic electrophile (Figure 1). AMs catalyze, also with the aid of MIO, the interconversion between α- and β-phenylalanine (β-Phe) or α- and β-tyrosine [phenylalanine aminomutases (PAMs) and tyrosine aminomutases (TAMs), respectively; Figure 1b].

The physiological functions of MIO-enzymes are diverse and constitute key roles in several metabolic pathways. In most kingdoms of living organisms, histidine ALs (HALs) play a crucial role in histidine metabolism.[2,3] Further, MIO-enzymes produce secondary metabolites such as antibiotics[4] or pigments[5] in bacteria and fungi. In plants, phenylalanine ALs (PALs) catalyze the carbon flow from the shikimate pathway to the phenylpropanoid pathway, leading to an enormous array of secondary metabolites such as lignins or flavonoids.[6] Due to the fundamental role of the phenylpropanoid pathway in plant metabolism, PAL is of key current interest.[6]

The application possibilities of MIO-enzymes are manifold, ranging from synthetic biotransformations to human therapy. The native promiscuity and wide substrate scope of numerous MIO-enzymes expedite their use as biocatalysts on laboratory as well as on industrial scale.[1,7] The enzyme substitution therapy with PAL for the treatment of phenylketonuria represents a further extension of applications.[8] In 2018, the FDA approved the first such treatment under the name Palynziq by BioMarin Pharmaceutical Inc.[9] Further development and fine-tuning of such important applications require a comprehensive understanding of the reaction mechanism and of the structure−function relationships of MIO-enzymes.

Different reaction mechanisms proposed for the AL reaction suggested different roles for the MIO electrophile (Figure 1a).

Received: January 19, 2021
Revised: March 17, 2021

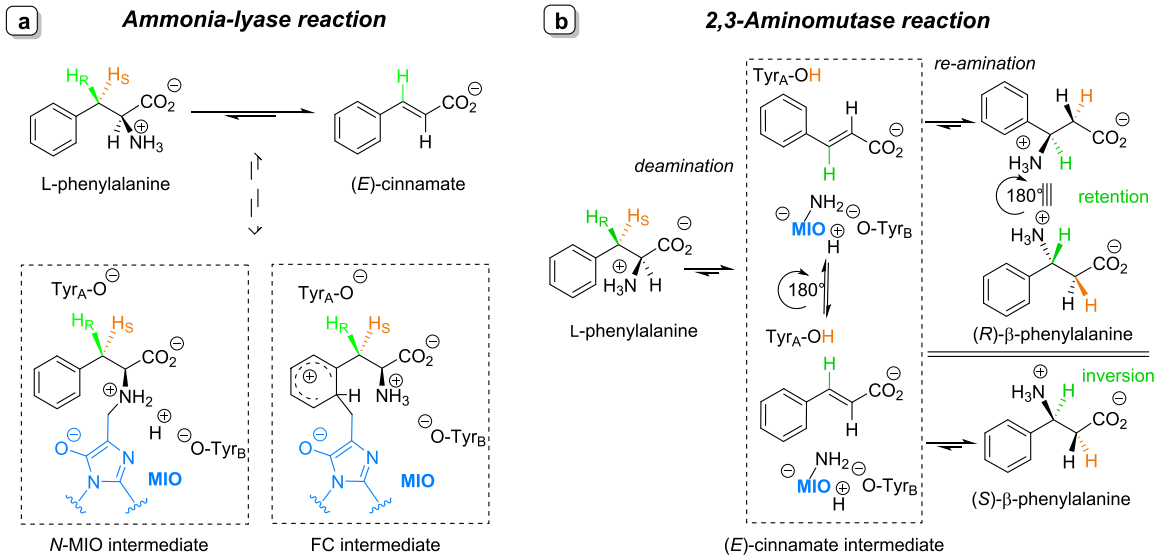

Figure 1. Catalytic activity and key structural features of MIO-enzymes. The AL reaction (a) involves a covalent intermediate. In the proposed N-MIO intermediate, a bond is formed between the amino group of the substrate and the exocyclic methylene carbon atom of the MIO electrophile. In the alternative hypothetic Friedel–Crafts (FC) intermediate, the MIO electrophile forms a σ-complex with the phenyl ring of the substrate. In different AM reactions (b), after forming an amino–MIO complex and a cinnamate, the re-amination steps result in different enantiomers of the β-amino acid via "inversion of configuration" or "retention of configuration" routes. The routes are named depending on whether the configuration of the *pro-R* β-hydrogen (in green) of the starting L-Phe is formally retained or inverted. During the AM reactions, the *pro-S* β-hydrogen (in orange) is shifted to the α-carbon atom.

The N-MIO mechanism postulated an N-MIO intermediate by covalent bond formation between the amino group of the substrate and the exocyclic methylene carbon atom of the MIO electrophile.[10] The FC mechanism hypothesized an FC intermediate resembling the σ-complex involved in FC reactions by covalent bond formation between the aromatic moiety of the substrate and the exocyclic methylene carbon atom of the MIO electrophile.[11,12] Both the N-MIO and Friedal–Crafts (FC) mechanisms suggested that a tyrosine residue (Tyr_A in Figure 1) plays the role of the catalytic base responsible for removing the *pro-S* hydrogen (H_s) as a proton from the β position during the elimination reaction.[13]

Different reaction routes in the PAM reaction result in mirror-image enantiomers of β-Phe (Figure 1b). Isotope labeling studies revealed that eukaryotic PAMs convert L-α-phenylalanine (Phe) to enantiopure (*R*)-β-Phe via the "*retention of configuration*" route[14] (referring to the *pro-R* β-hydrogen of the substrate, depicted in green in Figure 1b). In contrast, prokaryotic PAMs transform Phe to enantiopure (*S*)-β-Phe via the "*inversion of configuration*" route[15] (Figure 1b). In both AM routes, the *pro-R* β-hydrogen is shuffled as a proton by Tyr_A to the α position, whereas the amino group transfer is mediated by the MIO group. Independently from their origin, TAMs exhibit no strict preference toward either enantiomers of β-tyrosine (β-Tyr).[4,16] So far, all hypotheses on the mechanisms for the AM reactions postulated the existence of the unsaturated carboxylic acid intermediate[1] (e.g., (*E*)-cinnamate (CA), the respective intermediate for PAMs). Another common feature of all AM reactions is the release of this unsaturated carboxylic acid intermediate as a by-product,[17,18] presumably as a result of the intermediate's egress from the active site prior to re-amination. Notably, this intermediate is equivalent to the product of the AL reaction.

In all MIO–enzymes (Table S1) Tyr_A is present in a conserved sequence motif part of a flexible inner loop covering the active site (Table S2 shows a sequence alignment of the region). The catalytically competent conformation of the inner loop is characterized by the proper spatial proximity of Tyr_A to MIO (~12–13 Å, Figure 2). The representative crystal

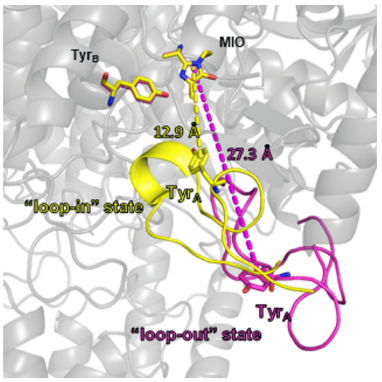

Figure 2. Spatial proximity of TyrA to MIO in the "loop-in" state (yellow; in structure 6F6T) of the inner loop within PcPAL allows the catalytic activity. In the "loop-out" state assumed for PcPAL previously (magenta; in structure 1W27),[30] however, TyrA lies far away from the active site and cannot fulfill the role of being the catalytic base.

structures of each class of MIO–enzymes[3,4,8,18−33] show clear-cut electron densities for the well-ordered inner loop conformation in the so-called "loop-in" state (Figures 2, S1 and S2), except for eukaryotic PALs.[8,20,21,32,33] The lack of proper electron density data hindered modeling the loop region in the crystal structures of PAL from the yeast *Rhodotorula toruloides*.[8,20] The inner loop is also absent in our recent structure of *Petroselinum crispum* PAL (PcPAL, I460V mutant) despite the presence of *p*-methoxy cinnamic acid ligand in the active sites.[33] In the first structure of PcPAL, a "loop-out" conformation was assumed for the inner loop[21] (Figure 2); however, this conformation proved to be catalytically

https://doi.org/10.1021/acscatal.1c00266
ACS Catal. XXXX, XXX, XXX−XXX

inactive.[34] In the recent structure of *Sorghum bicolor* PAL, the inner loop of chain A was resolved in a "loop-in" state,[32] but modeling of this region is still ambiguous due to the low resolution (2.5 Å) and weak electron densities for the side chains in the inner loop region.

The inner loop in PAM is rendered more rigid than the one in PAL by a combination of salt bridges[35] and hydrophobic interactions.[18] Computational and experimental results suggested the difference in flexibility of the inner loop to be the key structural feature distinguishing ALs from AMs.[18,35] Thus, it was proposed that the more rigid loop in PAM restrained the CA and the amino-enzyme (NH_2-MIO) intermediates within the active site during isomerization. Mutating several hydrophobic residues of the inner loop in the (*R*)-selective *Taxus canadensis* PAM (TcPAM) to their more hydrophilic equivalents in PcPAL resulted in an AL phenotype, and computational results demonstrated that the mutations also lowered the potential mean force required for loop opening.[18] However, both studies assumed that a transition from the "loop-in" state of the inner loop to the "loop-out" state (Figure 1) occurs during the catalytic cycle.[18,35] Furthermore, in an independent study, the reverse experiment aiming to switch the AL to AM activity was unsuccessful.[36]

Currently, strong structural evidence for the catalytic mechanism and substrate binding is lacking for eukaryotic PALs being crucial in plant metabolism. Therefore, the first goal of this study was to determine the catalytically competent structure of a eukaryotic PAL (PcPAL). The second goal of this study was to investigate the dynamic behavior of a eukaryotic PAL and a PAM during substrate binding/product release, with special focus on the conformational changes of the inner loop during the process. Subsequent mutagenesis of critical access tunnel residues aimed to alter the activity and/or stereopreference of PALs and PAMs.

RESULTS

X-ray Structures of PcPAL with Catalytically Competent Inner Loop Conformation. The crystal structures of PcPAL have been solved in apo form (PDB ID: 6H2O) and in complex with previously characterized potent phosphonic acid inhibitors (*R*)-(1-amino-2-phenylethyl)phosphonic acid [(*R*)-APEP, PDB ID: 6HQF] and (*S*)-(1-amino-2-phenylallyl)-phosphonic acid [(*S*)-APPA, PDB ID: 6F6T][37] (Figure 3). Table S3 lists the details of data collection and structure refinement.

Co-crystallization with 10-fold excess of (*R*)-APEP or (*S*)-APPA resulted in full occupancy of the active sites of PcPAL (Figure 3a,b). In the structures, both (*R*)-APEP and (*S*)-APPA are covalently attached to the MIO residue by their amino group, despite the reversibility of the inhibition[37] (Figure 3c: *N*−*C* distances are 1.3 and 1.4 Å for (*R*)-APEP and (*S*)-APPA, respectively). The inhibitor (*R*)-APEP is the phosphonic acid equivalent of the natural substrate L-Phe; hence, the binding conformation and the reaction mechanism of the AL reaction with L-Phe may be inferred from this crystal structure. The binding conformation is equivalent to the N-MIO intermediate state proposed for the reaction (Figure 1a). As such, these structural data provide the first direct experimental evidence for the N-MIO mechanism for PALs (Figure 1a). Furthermore, the experimental evidence shows (*R*)-APEP to be a mechanism-based inhibitor that mimics an intermediate state of the reaction. However, the elimination reaction from this

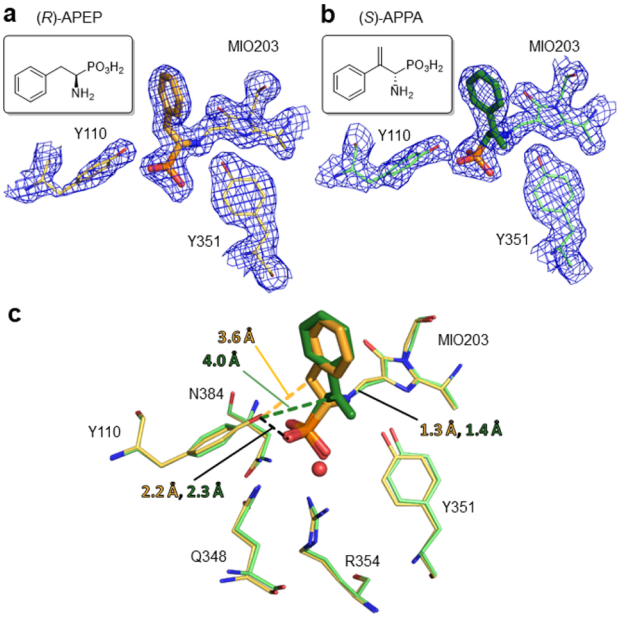

Figure 3. Covalent binding of mechanism-based phosphonic acid inhibitors of PcPAL. (a,b) Clear electron densities indicate covalent bonds between the catalytic MIO residue of PcPAL and the ligands (*R*)-APEP (a) and (*S*)-APPA (b). (c) Comparative overlay of the inhibitor-binding modes of PcPAL. The distance between the amino group of the inhibitors and the exocyclic methylidene group of the MIO residue is characteristic of a covalent bond: 1.3 Å in (*R*)-APEP and 1.4 Å in (*S*)-APPA. Electron densities are shown from the 2Fo−Fc maps, contoured at 1σ level.

inhibitor cannot occur, as the essential base Tyr_A (Y110, Figure 3) forms a salt bridge with the phosphonic acid moiety.

The clear-cut electron densities in the structure complexed with the inhibitors confirm the absolute configuration determination of the (*S*)-APPA inhibitor (Figure 3b) and reveal a surprising enantiomer preference switch generated by the methylidene group in (*R*)-APEP at the β-position (Figure 3b).[37] Inferring D-Phe binding from this structure, we propose that the positioning of the β-carbon atom compared to Tyr_A (Y110, Figure 3c) is the most important structural feature determining enantioselectivity.

PcPAL, like all MIO–enzymes, functions as a homotetramer.[38] Each of the four active sites of the tetramers is formed by three monomers,[3] and the burial of large hydrophobic surfaces between the subunits is the driving force of tetramerization. In all of the crystal structures reported here, PcPAL crystallized in the same unit cell as in the previously reported structures.[21,33] The asymmetric unit consists of two monomers, and the functional homotetramer is generated by applying crystal symmetry operations. The overall protein fold well represents the usual MIO–enzyme fold;[3,4,8,18−33] however key details are also revealed by the present structures. Inhibitor binding decreased the flexibility of the inner loop and the experimental electron density maps, allowing the creation an unequivocal structural model of the inner loop region as well (Figure 4).

The inner loop region (106−126, Table S2) directly caps the active site, encompasses the catalytic Tyr_A (Y110), and is stabilized upon ligand binding. In the apo structure, electron densities for the inner loop were absent, presumably due to the higher flexibility of the loop (Figure 4a). Binding of the inhibitors (*R*)-APEP and (*S*)-APPA resulted in structures with

https://doi.org/10.1021/acscatal.1c00266
ACS Catal. XXXX, XXX, XXX−XXX

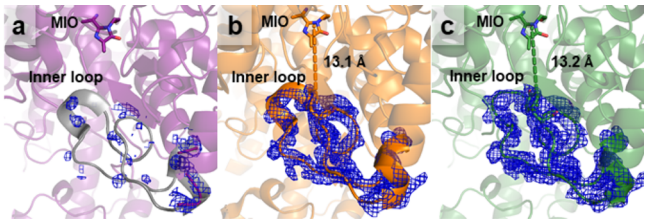

Figure 4. Reaction intermediate mimicking inhibitor binding stabilizes the inner loop in PcPAL crystal structures. A close-up view of the inner loop capping the active site, with highlighted electron densities, is shown in the blue mesh. Electron densities are absent in the apo PcPAL structure (a, 6H2O; the loop conformation in the other PcPAL structures is shown in gray). The inner loop is unambiguously visible in the electron density maps for the PcPAL structures complexed with (*R*)-APEP and (*S*)-APPA[37] [(b) 6HQF and (c) 6F6T, respectively]. Electron densities are shown from the 2Fo−Fc maps, contoured at 1σ level.

clearly visible electron densities for the inner loop, allowing accurate modeling of the full inner loop for the first time for a eukaryotic PAL (Figure 4b,c). In this inner loop conformation, the Tyr_A−MIO distance (13.2 and 13.1 Å, Figure 4b,c) enables the action of Tyr_A as the catalytic base and therefore can be considered a catalytically competent conformation. This conformation of the inner loop resembles the "loop-in" state seen in other MIO-enzymes (structural overlay shown in Figure S2a). Importantly, no experimental data support the previously proposed "loop-out" state,[21] rendering the functional relevance of this conformation questionable. The strong interactions of the phosphonic acid moiety of the reaction intermediate mimicking analogues with multiple active site residues likely contribute to the stabilization of the Tyr_A-containing inner loop, as no such effect was observed even in the PcPAL structure complexed with a cinnamic acid analogue, enabling less stabilizing interactions.[33]

Inner Loop Dynamics in PcPAL and TcPAM during Substrate Access and Product Release. In MIO-enzymes, it was often assumed that the inner loop undergoes large conformational changes and fully opens approaching the hypothetical "loop-out"[21] conformation upon product release.[18,35] The crystallographic experimental evidence, however, only proved unambiguously the existence of the "loop-in" state in PcPAL. Additionally, inner loop flexibility was suggested to switch between PAL and PAM activities.[18] The role of inner loop motions in distinguishing PAL and PAM reactions was studied by modeling the loop motions of a eukaryotic PAL and a eukaryotic PAM during substrate binding and product release.

The structures of PcPAL, with the complete inner loop in a catalytically competent "loop-in" state, and the available structures of TcPAM enabled us to set up random acceleration molecular dynamics (RAMD)[39] simulations. As RAMD requires no prior assumption of the dissociation pathway, it is a powerful tool for investigating ligand egress routes from buried binding sites.[40,41] Thus, RAMD was applied to study the ligand egress pathways and inner loop dynamics upon ligand egress in full tetrameric models. It is well established that both PcPAL[37] and TcPAM[35] bind and react with Phe and

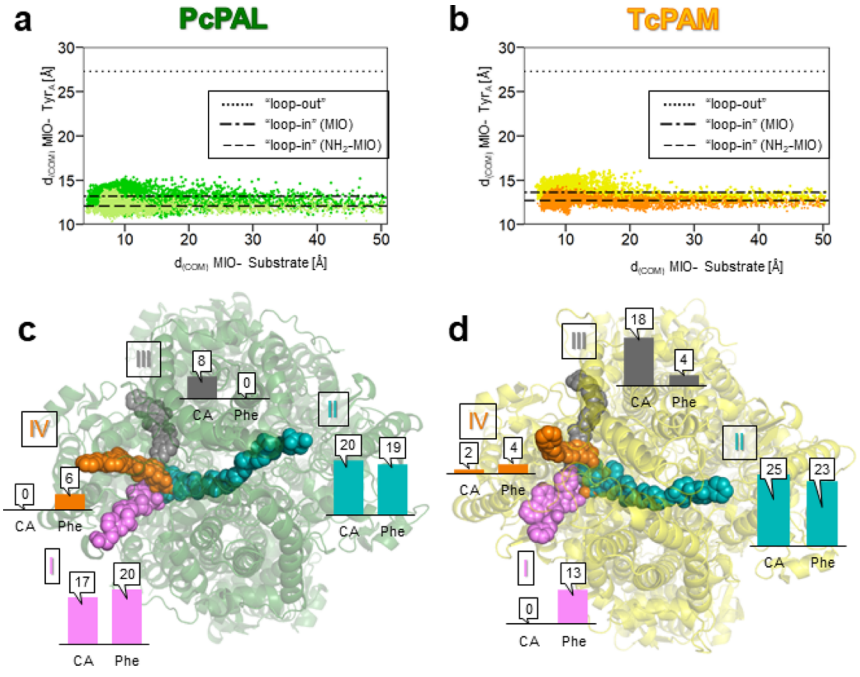

Figure 5. Ligand egress dynamics in PAL and PAM models. Inner loop opening in PcPAL (a) and TcPAM (b), characterized by the Tyr_A−MIO distance as a function of ligand egress. The *x*-axis shows the distance between the COM of the ligand and MIO and the *y*-axis shows the distance between the COM of Tyr_A and MIO. Each plot shows aggregated data from 90 RAMD simulations. Dots in green represent data from the simulations of PcPAL with Phe and dots in lime represent simulations with CA (a). Dots in yellow represent data from simulations of TcPAM with Phe and dots in orange represent simulations with CA (b). Dashed and dotted dashed lines show Tyr_A−MIO COM distances in the "loop-in" conformations in the crystal structures (6F6T for PcPAL and 2YII for TcPAM[28]). Dotted lines show the Tyr_A−MIO COM distance in the "loop-out" conformation of 1W27.[21] (c) Exit paths observed in PcPAL. (d) Exit paths observed in TcPAM. One representative path is depicted for each observed pathway in both models. Bar graphs show the number of occurrences for the exit paths in the independent RAMD simulations for the two ligands CA and Phe.

https://doi.org/10.1021/acscatal.1c00266
ACS Catal. XXXX, XXX, XXX−XXX

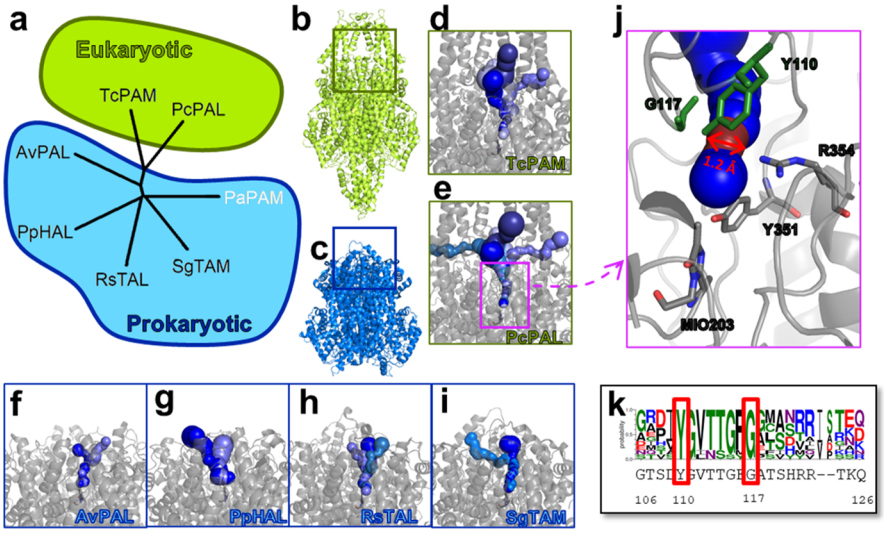

Figure 6. Initial part of path II in PcPAL and TcPAM coincides with the conserved tunnels in different classes of MIO-enzymes. a, Phylogenetic relationship of the archetypal MIO-enzymes. In the tetrameric structures of MIO-enzymes from eukaryotes (b) or prokaryotes (c), tunnel analysis revealed a highly conserved tunnel connecting the active site to the surface of the protein in *T. canadensis* PAM [(d) PDB ID: 2YII)],[28] *P. crispum* PAL [(e) PDB ID: 6F6T], *Anabaena variabilis* PAL [(f) PDB ID: 3CZO],[25] *Pseudomonas putida* HAL [(g) PDB ID: 1GKM)],[19] *Rhodobacter sphaeroides* TAL [(h) PDB ID: 2O6Y)],[22] and *Streptomyces globisporus* TAM [(i) PDB ID: 2QVE)].[24] Spheres colored to different shades of blue represent distinct tunnels within the structures. The starting part of the exit path from the MIO until the bottleneck position (j) is highly homologous in space in both eukaryotic (b) and prokaryotic (c) MIO-enzymes, despite the large structural differences in the C-terminal multihelix domains. Sequence analysis of the inner loop of the MIO-enzymes (k) revealed that the bottleneck position is related to the fully conserved Tyr110 and Gly117 residues (PcPAL numbering). In the structure of *Pantoea agglomerans* PAM (3UNV),[29] the tunnel analysis tool could not detect any tunnel connecting the active site to the surface of the enzyme.

CA. Therefore, our RAMD simulations investigated the release of both Phe and CA, assuming that their binding/release occurs via the same paths. The distance between the center of mass (COM) of the catalytic Tyr_A (Tyr110 in PcPAL, Tyr80 in TcPAM) and that of the MIO residue served as a measure of the inner loop opening, in accordance with the previous study of Heberling et al.[18]

The MD simulations revealed that the inner loop persisted in its ~~closed~~ "loop-in" state during the egress of either Phe or CA from the active site (Figure 5a,b). None of the models transitioned to the "loop-out" conformation, as the MIO−TyrA distances remained at the same low level associated with the "loop-in" state. Furthermore, no loop opening was detected in PcPAL or TcPAM with either ligand (Phe or CA) beyond regular movements observable in the other active sites of the tetrameric models (Figures S3 and S4). Therefore, the crystallographic evidence combined with the RAMD results rule out the biological relevance of the "loop-out" conformation of the inner loop.

Visual clustering of ligand egress paths revealed four distinct ligand access pathways in PcPAL (Figure 5c). Four highly homologous paths occurred in TcPAM (Figure 5d) as well, suggesting that substrate access paths are conserved in eukaryotic PALs and PAMs. Path I (pink) led between the inner loop and another flexible loop capping the active site (sometimes referred as outer loop). This pathway was previously suggested as an access to the active site, based on static crystallographic data.[4,21] Statistical data corroborate the previous hypothesis (Figure 5c,d: bar graphs), as this path was frequently observed in the RAMD simulations. However, MD data revealed three additional egress/access paths from/to the active site. Path II (blue) progressed through the C-terminal multihelix domain. Occurrence frequencies suggested path II to be the most frequented egress route in PcPAL as well as in TcPAM. Path III (gray) proceeded through the hydrophobic part of the binding pocket, whereas path IV (orange) led through a turn in the inner loop. These two pathways were seldom taken by the ligands, suggesting that they have only a minor biological role, or they are just simulation artifacts.

Identification of the Conserved Ligand Access Tunnel within the MIO-Enzyme Family. In silico tools proved to be useful to uncover tunnels in crystal structures connecting the buried active sites with the solvent-exposed outer surface of the protein in several enzyme families such as cytochrome enzymes[42] and dUTPase.[41] There are many examples of tunnels important for protein function, including the effect of mutations on tunnel anatomy/function. Changes in the access tunnels can influence the activity, specificity, stability, or even enantioselectivity of an enzyme.[43]

Inspired by the conservation of the ligand egress pathways in eukaryotic PAL and PAM, we further widened these studies to include the experimental structures of all archetypal MIO enzymes (Figure 6a).

Eukaryotic MIO-enzymes (Figure 6b) contain ~~200~~ additional residues at their C-terminal compared to the MIO enzymes of prokaryotic origin (Figure 6c). Tunnel analysis of PcPAL and TcPAM revealed that the newly discovered path II (Figure 5c,d) coincided with a conserved tunnel connecting the active site to the surface of the protein through the C-terminal multihelix domain (Figure 5d,e). This corroborated the biological relevance of path II and indicated that tunnel-finding algorithms like MOLE[44] or CAVER[45] may constitute suitable tools for finding such paths.

In the prokaryotic MIO-enzymes, the conserved ligand access paths (Figure 6f−i) show architecture that is highly similar to the common initial part of path I and path II (Figure 6d,e) identified within the eukaryotic MIO-enzymes (Figure 6b). This conserved part of the tunnels leads through a

https://doi.org/10.1021/acscatal.1c00266
ACS Catal. XXXX, XXX, XXX−XXX

bottleneck position defined by Tyr110, Gly117, and Arg354 (Figure 6j), which are strictly conserved within all MIO enzymes (Figure 6k and Table S2), indicating a potential evolutionary gatekeeper role of these residues. Moreover, this tunnel was the only one with larger than 1.1 Å inner sphere size connecting the active site with the surface of the protein in all the investigated MIO-enzymes. The structural characteristics of the inner and outer loops capping the active sites together with the access tunnel data suggest that path I and path II constitute the major substrate access and product release pathway not only in PcPAL and TcPAM but in all MIO enzymes.

The active site of prokaryotic (*S*)-PAMs (archetype: *Pantoea agglomerans* PAM, PaPAM) is the most shielded from the surface of the protein; no tunnels with larger than 1.1 Å diameter can be detected in the structure. Both path I and path II appear to be blocked in PaPAM by residues being conserved only within prokaryotic (*S*)-PAMs.[29] In the structure of PaPAM, a glutamine to glutamic acid substitution at position 317 (Figure S5) forms a strong salt bridge to Arg323 and thereby blocks path I. Path II, a conserved tunnel in other MIO enzymes (Figure 6), is narrowed in (*S*)-PAMs by the mutation of asparagine to a bulkier phenylalanine at position 455 (Figure S5.). This agrees with the proposed mechanism of (*S*)-PAMs (Figure 1b), indicating the necessity of "caging" the intermediate state of isomerization without serious movements of the ligand within the active site.

Mutagenesis of Critical Access Tunnel Residues to Tailor PAL and PAM Activities. We postulated that narrowing the exit path I and/or II of PALs or (*R*)-PAM by appropriate mutations of critical tunnel residues mimicking those observed in (*S*)-PAMs could enhance the (*S*)-PAM activity. Single and double mutants (Figure S5) were created from a eukaryotic PAL (PcPAL), from a prokaryotic PAL (*Kangiella koreensis* PAL, KkPAL[46]), and from a eukaryotic (*R*)-PAM (TcPAM). Reactions starting from L-*α*-Phe, racemic *β*-Phe, and CA evaluated the full spectrum of AL and AM activities, by following the changes in *α*-Phe, *β*-Phe, and CA quantities as a function of time for 168 h. Parallel measurements of reactions with *Pseudomonas fluorescens* PAM (PfPAM)[47] served as controls for the (*S*)-PAM reactions.

Unsurprisingly, sealing either or both substrate-binding tunnels in a eukaryotic PAL or in a prokaryotic PAL did not create detectable AM or *β*-AL activity (Figures S6–S8). Interestingly, in the reactions starting from L-*α*-Phe with wild-type TcPAM, the amount of the AM reaction product decreased after an initial buildup, and the AL product, CA, accumulated after prolonged reaction times (Figures S6–S8). This is probably the result of the trace AL activity and the strongly shifted equilibrium of the AL reaction toward CA formation from Phe. In contrast, the PfPAM-mediated transformation of L-*α*-Phe revealed dominant AM activity even after a prolonged reaction time (Figure S9).

In contrast, all the TcPAM mutants gained the ability to convert (*S*)-*β*-Phe (see Figures S6–S8 displaying the progress curves of the reactions starting from L-*α*-Phe, racemic *β*-Phe, and CA, respectively; Tables 1 and S4 containing the conversion and enantiomeric composition data in various biotransformations; and Figures S10–S13 displaying representative HPLC chromatograms). Mutation TcPAM N458F, influencing the initial part of path II, affected the enantiomeric preference the least. In the reaction starting from *α*-Phe, TcPAM N458F displayed not only significant *α*-AL but also AM activity. In the reaction that started from ~~*rac*~~-*β*-Phe, the N458F mutant exhibited a weak and slightly (*R*)-selective *β*-AL activity and a fully suppressed AM activity. In agreement, this mutant converted CA in the ammonia addition to a mixture of (*S*)-*α*-Phe and (*R*)-*β*-Phe after 168 h.

Table 1. Biotransformations of Racemic *β*-Phe with TcPAM Constructs after 168 h[a]

	β-Phe[a]			
TcPAM variant	*c* [%]	config.	ee_s [%]	*E*[b]
TcPAM wt	40.9	*S*	94.3	n.d.[c]
TcPAM N458F	22.8	*S*	16.8	4
TcPAM Q319E	36.0	*S*	4.5	1
TcPAM Q319E/N458F	40.8	*R*	61.1	31

[a] *c*: conversion; config.: configuration of the residual *β*-Phe fraction; ee_s: enantiomeric excess of the residual fraction of the ~~*rac*~~-*β*-Phe substrate. [b] Enantiomer selectivity (*E*) in kinetic resolutions by an irreversible reaction was calculated, as defined by Sih and co-workers:[48] $E_{c,ee_s} = \ln[(1 - c)(1 - ee_s)]/\ln[(1 - c)(1 + ee_s)]$. [c] Not determined because the enantiomer selectivity (*E*) interpreted by the above formula is valid only for irreversible reactions (the wt-TcPAM-mediated reactions are reversible even in the presence of trace amounts of ammonia).

Mutation TcPAM Q319E, influencing the initial part of path I, altered the stereopreference of *β*-Phe enantiomers more significantly, exhibiting almost equal preference for both enantiomers. The Q319E mutation significantly decreased the enzyme activity in the reaction that started from L-*α*-Phe, and only a minimal formation of the AM reaction product along with the AL product could be detected after 168 h. Contrarily, when the reaction started from *rac*-*β*-Phe, TcPAM Q319E produced 36% CA, but no AM activity was observed. The nonselective conversion of racemic *β*-Phe means a significant activity increase toward (*S*)-*β*-Phe as compared to the wild-type enzyme. Inspecting the viability of the same mutant in the ammonia addition reaction onto CA, only a total conversion of 3% to *β*-Phe was revealed after 168 h.

The TcPAM Q319E/N458F double mutant became an apparent (*S*)-*β*-AL as it showed the highest conversion of *rac*-*β*-Phe to CA, leaving (*R*)-*β*-Phe after 168 h. Consequently, the Q319E/N458F TcPAM consuming (*S*)-*β*-Phe with significant enantiomer selectivity may be considered a highly selective (*S*)-*β*-AL. Importantly, the double mutant TcPAM Q319E/N458F produced solely (*S*)-*β*-Phe in the addition reaction starting from CA after 168 h, indicating the high (*S*)-enantiopreference of the double mutant in the reverse *β*-AL direction as well.

Overall, the introduction of any of the path-sealing (*S*)-PAM-like residues to TcPAM significantly decreased the AM activity and strongly hindered the mediation of ammonia addition to CA. In line with our initial assumptions, the mutation of only two residues (Q319E and N458F) could impair or even alter the stereoselectivity of the strictly (*R*)-selective TcPAM. Of the two mutations in TcPAM, the enantiomer selectivity-altering effect of Q319E TcPAM was more pronounced. Presumably, both the access tunnel modification and the involvement of Q319 in the binding of the substrate's carboxylate group can be involved in the alteration effect. The synergistic effect of the two mutations rendered the double mutant TcPAM Q319E/N458F acting as an (*S*)-*β*-AL representing a nonassigned enzymatic function.

https://doi.org/10.1021/acscatal.1c00266
ACS Catal. XXXX, XXX, XXX−XXX

DISCUSSION

A wealth of evidence has already supported the mechanism through an N-MIO intermediate (Figure 1a) in different MIO enzymes;[1,13] however, until now, there was no direct demonstration of the formation of the N-MIO intermediate in the PAL reaction. Earlier, due to the weak acidity of the β-hydrogen atoms, a FC-like mechanism involving an electrophilic attack of the MIO catalytic residue at the aromatic ring of the substrate was also proposed for the HAL[49] and PAL[11] reactions. Later, the crystal structure of RsTAL showed the AIP inhibitor to be covalently bound via its amino group to MIO, supporting the N-MIO mechanism for TALs.[22] The quantum mechanics/molecular mechanics studies also confirmed the N-MIO mechanism for RsTAL from a theoretical aspect.[13] To consolidate the two reaction mechanisms, it was suggested that TAL/TAM enzymes use the N-MIO mechanism, whereas PAM/PAL enzymes use the FC mechanism.[50] However, kinetic isotope effects indicated the N-MIO mechanism for (*S*)-β-selective PAM,[15] and later, the crystal structure of a PaPAM binding both α- and β-Phe covalently via their amino groups to MIO provided the direct support of the N-MIO mechanism for PAMs.[29] PcPAL was also shown to catalyze ammonia elimination from nonaromatic substrates, propargylglycine,[51] styrylalanine,[52] or cyclooctatetraenylalanine,[53] necessarily favoring the N-MIO mechanism; however, direct structural evidence supporting the N-MIO mechanism for PALs has not been published yet. The crystal structures, especially PcPAL complexed with the phosphonic acid analogue of the natural substrate, (*R*)-(1-amino-2-phenylethyl)phosphonic acid (PDB ID: 6HQF), presented in this work fill this gap and provide direct evidence for the N-MIO mechanism for PALs. Based on the above arguments, it is almost certain that reactions of all MIO-enzymes proceed by mechanisms involving the N-MIO intermediate, despite the absence of direct structural evidence for HALs.

A hypothesis suggested that the altered flexibility of the inner loop is responsible for the AL versus AM activity switch.[18,35] Mutagenesis results supported the hypothesis, as enhancing the flexibility of the inner loop of TcPAM resulted in AL phenotype.[18] The theory has been strongly based on the structure 1W27[21] with its inner loop in the "loop-out" conformation. However, this state is ambiguous due to the weak electron density for this loop region and poor fit of the modeled loop to the electron density map (Figure S1). The crystal structures, 6F6T and 6HQF, showed for the first time in a eukaryotic PAL structure well-defined electron densities that enabled the determination of the catalytically competent "loop-in" conformation for the inner loop. A series of RAMD simulations within PcPAL and TcPAM models revealed only small changes in inner loop conformations, allowing the egress of ligands from the active site of both enzymes. These results agree with the "*principle of least motion*" for organic reactions,[54,55] which seemed to be generalizable to enzyme-catalyzed reactions as well.[13,56,57] Together, the lack of crystallographic evidence and the RAMD results call into question the actual formation and biological significance of the "loop-out" conformation of the inner loop. The altered loop flexibility hypothesis is weakened by the failure of efforts to convert an AL to AM by reverse mutagenesis, attempting to increase the rigidity of the inner loop to introduce the AM function.[36] Moreover, the loop flexibility hypothesis cannot explain the regioselectivity difference between ALs and AMs in the reverse reaction: while ALs result in α-amino acids solely,[1,7] AMs always produce a mixture of α- and β-amino acids.[35] Furthermore, our results also indicated that loop flexibility differences can only partially explain the differences between ALs and AMs.

Aiming at the development of more active biocatalysts and the fundamental understanding of MIO-enzymes, several studies investigated the molecular basis of the activity differences between ALs and AMs. The effect of mutating the substrate-orienting residues on AM activity was explored, and it mostly resulted in a decrease in AM activity. Mutating E239 in *Streptomyces maritimus* PAM (SmPAM) to Gln or Met shifted the addition reaction to the α direction, whereas the enantioselectivity remained unaltered.[58] We found that the equivalent reverse mutation Q319E in TcPAM resulted in significantly decreased activity in the addition reaction but retained an AL and some AM activity for both α- and β-Phe. Mutation of Q319M in TcPAM resulted in enhanced (*R*)-β-Phe production in the addition reaction (88%:12% β/α-Phe product).[28] Two independent studies showed that mutating F455 in PaPAM to Asn or Ala resulted in a significantly reduced reaction rate when started from α-Phe and in a decreased production of β-Phe and in an increased production of CA.[29,59] The authors explained the decreases in the β-products by the substrate-orienting effects of these residues. The reverse N458F mutation in TcPAM resulted in an enhanced (*R*)-β-Phe production in the ammonia addition reaction (85%:15% β/α-Phe product).[60] Although the N458F mutation in our experiments significantly decreased the rate of the addition reaction, our TcPAM N458F mutant displayed enhanced activity toward β-Phe, compared to that found for the transformation of α-Phe. The discrepancies concerning the already published conversion values for the PAM-mediated ammonia addition reactions can be mostly attributed to the wide variety of the used reaction medium (ammonia concentration, type of buffers, pH, etc.). Nonetheless, the biocatalytic performances of the (*R*)-selective wt-TcPAM and of the (*S*)-selective wt-PfPAM checked by us in the ammonia addition reactions were in good concordance with those already reported.[28,47]

Remarkably, only marginal efforts have been dedicated at investigating the molecular background and engineering of the enantioselectivity of MIO-enzymes. ALs show virtually perfect enantioselectivity for their natural substrates.[61] The different types of PAM also show perfect enantioselectivity to either (*R*)-β-Phe[14] or (*S*)-β-Phe.[15] However, prokaryotic TAMs produce a mixture of (*R*)-and (*S*)-β-Tyr.[4,16] On the other hand, enantioselectivity of MIO-enzymes for non-natural substrates is highly variable.[58] Our previous study showed that the methylidene group at the β-position in APPA altered the enantiopreference of binding of this phosphonic acid analogue of Phe in PALs.[37] Our recent set of experiments introducing the binding pathway-blocking residues from the (*S*)-selective PaPAM to the (*R*)-selective TcPAM indicated the potential of structure-based enzyme access tunnel engineering to alter the enantioselectivity of MIO-enzymes (Figure 6). The strict enantiomer preference of the (*R*)-selective TcPAM altered significantly in both the ligand access tunnel mutants of TcPAM, whereas the double mutant became an (*S*)-selective β-AL.

Previously, two main approaches have been used to modify AL and AM activities, namely, the loop flexibility modulation and substrate-binding modulation. In this study, a third

https://doi.org/10.1021/acscatal.1c00266
ACS Catal. XXXX, XXX, XXX−XXX

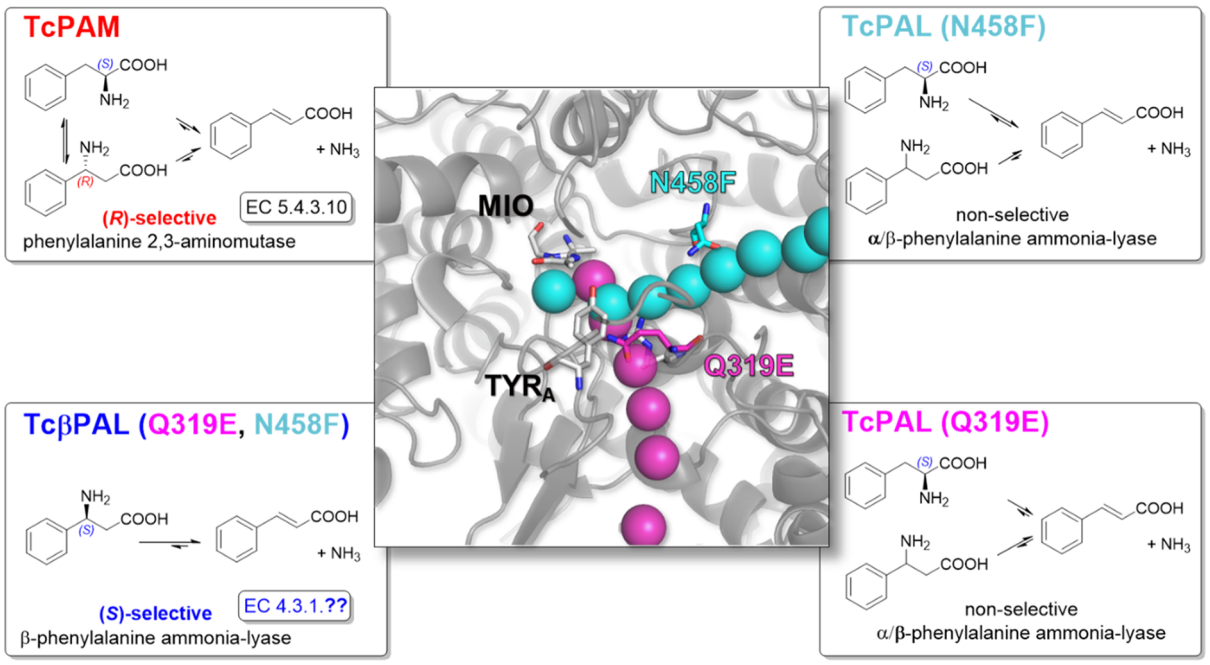

Figure 7. Substrate access tunnel engineering modulates PAM, PAL, and β-PAL activity and enantioselectivity in MIO-enzymes. Wild-type TcPAM catalyzes the interconversion between L-α-Phe, CA, and (R)-β-Phe. TcPAL (N458F) and TcPAL (Q319E) catalyze the ammonia elimination from L-α-Phe, (R)-β-Phe, and (S)-β-Phe. The most predominant activity of the double mutant of TcPAM (Q319E, N458F) is the selective ammonia elimination from (S)-β-Phe.

approach—the combined use of RAMD simulations and tunnel analysis—identified residues Q319 and N458 as potential gatekeepers of key substrate access tunnels and revealed the possibility of modifying AL and AM activities. Undeniably, the simulations and crystal structures unanimously showed that both Q319 and N458 play dual roles in the AL and AM reactions: substrate orientation during the reaction and modulation of substrate access channels. In fact, the single mutation Q319E alone or in synergistic cooperation with the N458F mutation generated TcPAM variants with shifted stereopreference toward (S)-β-Phe as the substrate. Residue Q319 is located in path I in the neighborhood of the active site of TcPAM, and most likely, it is also involved in the fixation of the substrate's carboxylate group. Thus, the altered carboxylate-binding mode due to the Q319E mutation could also contribute to the ability of the double mutant TcPAM Q319E/N458F to convert or form (S)-β-Phe in the ammonia elimination or in the ammonia addition reactions, respectively. It is quite possible that all MIO-enzymes hold the potential for α-AL, β-AL, (R)-AM, and (S)-AM activities, and their experimental observation depends on the relative rate of each reaction. For example, a recent study revealed the (S)-AM activity of a prokaryotic PAL after prolonged reaction times with non-natural substrates.[58]

The data summarized in Figure 7 represent how the different (S)-PAM-like ligand path-sealing mutations led from the (R)-selective TcPAM to the development of (S)-β-PAL activity, representing a nonassigned type of enzymatic activity. Although our original aim was to alter the binding dynamics and thus create an (S)-PAM from an (R)-PAM, the (S)-PAM-like ligand path-sealing mutations probably influenced the shape and catalytic abilities of the active site as well. The fact that the active site of TcPAM could accommodate (S)-β-AL activity as well underlines the versatility of the MIO-enzyme scaffold not just for substrate accommodation engineering but for enantioselectivity engineering as well. It is noteworthy that sealing access tunnels is not easy at all; in α/β-hydrolases, insertion of Cys−Cys bridge was the only, yet not perfect, way to seal the access tunnels by mutagenesis.[62]

In conclusion, we demonstrated that strongly binding inhibitors can stabilize the inner loop of a eukaryotic PAL in a catalytically competent conformation and provide key insights into understanding the reactivity and enantioselectivity of MIO-enzymes in general. MD simulations showed that ligand egress proceeds without a large-scale movement of the inner loop and indicated conserved ligand-binding tunnels within the protein family. We exploited tunnel engineering and constructed from an (R)-selective PAM an altered enzyme performing (S)-β-AL activity.[43] These results provide further evidence to the potential of the MIO scaffold to catalyze α-AL, β-AL, (R)-AM, and (S)-AM reactions and raise questions about the exact molecular mechanism of enantioselectivity in MIO-enzymes.

METHODS

Standard protocols used for cloning, site-directed mutagenesis, protein expression, and PAL and aminomutase activity measurements are detailed in Supporting Information Methods and Tables S5−S8. The enzyme activity measurements for the TcPAM variants were carried out at two different experimental locations, in Budapest and in Cluj-Napoca from biological replicates. The repeated experiments provided equal results for both the PAL and aminomutase activities.

Crystallization. Extensive trials of crystallization of PcPAL-His_{10} in the apo form were unsuccessful. Therefore, PcPAL-His_{10} solutions were supplemented with a 10-fold molar excess of (S)-APPA prior to crystallization. Crystals grew within weeks of setting up drops from a one-to-one mixture of the protein solution and the precipitant (14 w/v % PEG 6000,

https://doi.org/10.1021/acscatal.1c00266
ACS Catal. XXXX, XXX, XXX−XXX

HEPES 0.15 M pH 7.0), using the hanging drop vapor diffusion method with 2 μL drops.

Removal of His_{10}-tag significantly enhanced crystal formation, and numerous hits were obtained from the initial screens. Crystals for the diffraction experiments were grown using 20−26 w/v % PEG 3350 and potassium formate 0.1−0.3 M as a precipitant. Crystals of PcPAL in apo form grew within weeks of setting up drops from a one-to-one mixture of the protein solution and the precipitant, using the hanging drop vapor diffusion method with 1−3 μL drops.

Structure Determination. Diffraction dataset for 6F6T was collected at DESY Hamburg beamline MX2-P14, and datasets for 6H2O and 6HQF were collected in ELETTRA beamline 5.2R XRD1. XDS[63] was used for data processing. Structures were solved by molecular replacement by Phaser[64] using 1W27 as a starting model for 6F6T and with 6F6T as a starting model for 6H2O and 6HQF. Models were refined by PHENIX[65] and manually adjusted in Coot.[66] Data collection and refinement details are listed in Table S3.

Molecular Dynamics Simulations. Details for model establishments and MD simulations are described in the model preparation for molecular modeling and MD simulation sections of the Supporting Information. In the tetrameric models, four different states of the active site were probed: (A) RAMD model of ligand release, (B) ligand-bound state, (C) the enzyme state after ligand release (with MIO after Phe release and with NH_2-MIO after CA release), and (D) the apo state (see Table S9 for simulation details). During the RAMD simulations, only one active site (A) received an additional acceleration force; the other three (B−D) served as controls for the ground-state behavior of the enzyme. Prior to RAMD simulations, a short MD simulation ensured equilibration of the models (Figure S14) and determined the equilibrium behavior of the models. Protein flexibility is a key focus of this investigation; therefore, the appropriate modeling was also confirmed by comparing the crystallographic *B* factors to the root-mean-square fluctuation values in the MD simulations (Figure S15). Snapshots extracted from the MD simulations at 10 ns, 15 ns, and 20 ns served as starting conformations for the RAMD simulations.

RAMD Simulations. The RAMD[39] enhanced sampling method applies an artificial force to the substrate in a random orientation, accelerating the dissociation process.

First, optimal values were searched by RAMD runs with varied parameters for the acceleration of the substrate and for the minimum distance that the substrate must travel to keep the direction of the acceleration to set up the final RAMD simulations. Excessive acceleration or short distances will produce unnatural exit paths, whereas no exit will be observed during the desired timescale if the acceleration is too low. To obtain comparable results in the four models, the test simulations were run from all 12 starting structures with different setups. Acceleration and displacement settings were optimized to achieve exit times between 0.1 and 2 ns. Accelerations varied from 0.07 to 0.16 kcal mol^{-1} $Å^{-1}$ by 0.1 steps during the optimization. For the accelerations 0.10, 0.11, and 0.12 kcal mol^{-1} $Å^{-1}$, three displacement settings (0.1, 0.5, and 1 Å) were also assayed. Table S10 lists the parameter optimization results.

Finally, 15 independent RAMD simulations with 0.11 kcal mol^{-1} $Å^{-1}$ acceleration and 0.05 Å displacement settings were run from each of the three starting structures extracted from the MD simulations, resulting in 45 RAMD simulations for each of the four models.

Analysis of RAMD Simulations. Visual molecular dynamics[67] package was used for visual trajectory analysis. Tcl/Tk scripts measured the geometric parameters and movements in the trajectories. All data analyses were performed using R software.[68]

Tunnel Analysis in MIO-Enzymes. MOLEonline[44] was used for tunnel analysis within various MIO-enzyme structures. Residues Tyr_A and MIO were selected as the starting point of the tunnel. The probe radius was set to 3 Å, the interior threshold to 1.1 Å, and the minimum depth to 5.0 Å for the cavity search. The bottleneck radius was set to 1.1 Å for the tunnel search, and all advanced parameters were left at their default values.

■ ASSOCIATED CONTENT

Supporting Information

The Supporting Information is available free of charge at https://pubs.acs.org/doi/10.1021/acscatal.1c00266.

Additional experimental and modeling methodological details; protein production; mutagenesis; crystal structure determination; crystal structure analysis; kinetic measurements; molecular modeling; detailed HPLC methods; and example HPLC results (PDF)

■ AUTHOR INFORMATION

Corresponding Authors

Csaba Paizs − *Biocatalysis and Biotransformation Research Centre, Faculty of Chemistry and Chemical Engineering, Babeş-Bolyai University, RO-400028 Cluj-Napoca, Romania*; Email: csaba.paizs@ubbcluj.ro

Beáta G. Vértessy − *Institute of Enzymology, ELKH Research Center of Natural Sciences, H-1117 Budapest, Hungary; Department of Applied Biotechnology and Food Science, Budapest University of Technology and Economics, H-1111 Budapest, Hungary*; Email: vertessy.beata@vbk.bme.hu

László Poppe − *Department of Organic Chemistry and Technology, Budapest University of Technology and Economics, H-1111 Budapest, Hungary; Biocatalysis and Biotransformation Research Centre, Faculty of Chemistry and Chemical Engineering, Babeş-Bolyai University, RO-400028 Cluj-Napoca, Romania*; orcid.org/0000-0002-8358-1378; Email: poppe.laszlo@vbk.bme.hu

Authors

Zsófia Bata − *Department of Organic Chemistry and Technology, Budapest University of Technology and Economics, H-1111 Budapest, Hungary; Institute of Enzymology, ELKH Research Center of Natural Sciences, H-1117 Budapest, Hungary*

Zsófia Molnár − *Department of Organic Chemistry and Technology, Budapest University of Technology and Economics, H-1111 Budapest, Hungary; Institute of Enzymology, ELKH Research Center of Natural Sciences, H-1117 Budapest, Hungary*

Erzsébet Madaras − *Department of Organic Chemistry and Technology, Budapest University of Technology and Economics, H-1111 Budapest, Hungary; Institute of Enzymology, ELKH Research Center of Natural Sciences, H-1117 Budapest, Hungary*

https://doi.org/10.1021/acscatal.1c00266
ACS Catal. XXXX, XXX, XXX−XXX

Bence Molnár − *Department of Organic Chemistry and Technology, Budapest University of Technology and Economics, H-1111 Budapest, Hungary; Institute of Enzymology, ELKH Research Center of Natural Sciences, H-1117 Budapest, Hungary*

Evelin Sánta-Bell − *Department of Organic Chemistry and Technology, Budapest University of Technology and Economics, H-1111 Budapest, Hungary*

Andrea Varga − *Biocatalysis and Biotransformation Research Centre, Faculty of Chemistry and Chemical Engineering, Babeş-Bolyai University, RO-400028 Cluj-Napoca, Romania*

Ibolya Leveles − *Institute of Enzymology, ELKH Research Center of Natural Sciences, H-1117 Budapest, Hungary; Department of Applied Biotechnology and Food Science, Budapest University of Technology and Economics, H-1111 Budapest, Hungary*

Renzhe Qian − *Institute of Organic Chemistry, University of Vienna, A-1090 Vienna, Austria*

Friedrich Hammerschmidt − *Institute of Organic Chemistry, University of Vienna, A-1090 Vienna, Austria;* orcid.org/0000-0003-2193-1405

Complete contact information is available at: https://pubs.acs.org/10.1021/acscatal.1c00266

Author Contributions

Z.B. and Z.M. contributed to the work equally. Z.B., C.P., B.G.V., and P.L. designed the research. R.Q. and F.H. synthesized the aminophosphonic acid inhibitor. Z.B., B.M., and I.L. performed DNA manipulations; expressed, purified, and crystallized enzymes; and solved crystal structures. Z.B., Z.M., and E.M. produced the mutated proteins. Z.M and E.S.B. carried out the activity assays in Budapest, and A.V. carried out the activity assays in Cluj-Napoca. Z.B. and E.M. devised simulation strategies and performed and analyzed RAMD simulations. Z.B., B.G.V., and L.P. wrote the paper.

Notes

The authors declare no competing financial interest.

Protein X-ray structure data that support the findings of this study have been deposited in Protein Data Bank with the 6F6T, 6H2O and 6HQF accession codes (http://doi.org/10.2210/pdb6F6T/pdb, http://doi.org/10.2210/pdb6H2O/pdb, and http://doi.org/10.2210/pdb6HQF/pdb, respectively).

■ ACKNOWLEDGMENTS

The research reported in this paper and carried out at BME was supported by the NRDI Fund (TKP2020 IES, grant no. BME-IE-BIO) based on the charter of bolster issued by the NRDI Office under the auspices of the Ministry for Innovation and Technology (Budapest, Hungary). The National Research, Development, and Innovation Office (Budapest, Hungary) is acknowledged for funding (L.P.: SNN-125637 and L.P., B.G.V.: NRDI Office NKP-2018-1.2.1-NKP-2018-00005). L.P. and C.P. thank the financial funding for the project NEMSyB, ID P37_273, Cod MySMIS 103413 [funded by the Romanian Ministry for European Funds, through the National Authority for Scientific Research and Innovation (ANCSI), and co-funded by the European Regional Development Fund]. Competitiveness Operational Program 2014−2020 (POC) is also acknowledged. The authors also acknowledge the Gedeon Richter Talentum Foundation for the PhD fellowship of Z.M. Molecular simulations were supported by the computer cluster of BME (Budapest, Hungary; BME Superman) and High-Performance Cluster of the National Information Infrastructure Development Programme (Hungary; NIIF HPC). The European Synchrotron Radiation Facility (Grenoble, France; ESRF) and Elettra Synchrotron (Trieste, Italy) are also acknowledged for synchrotron data collection.

■ ABBREVIATIONS

AM, aromatic amino acid 2,3-aminomutase; AL, aromatic amino acid ammonia-lyase; CA, (*E*)-cinnamic acid; PAM, phenylalanine 2,3-aminomutase; PAL, phenylalanine ammonia-lyase; MIO, 5-methylene-3,5-dihydro-4*H*-imidazol-4-one

■ REFERENCES

(1) Parmeggiani, F.; Weise, N. J.; Ahmed, S. T.; Turner, N. J. Synthetic and Therapeutic Applications of Ammonia-Lyases and Aminomutases. *Chem. Rev.* **2018**, *118*, 73−118.

(2) Suchi, M.; Sano, H.; Mizuno, H.; Wada, Y. Molecular Cloning and Structural Characterization of the Human Histidase Gene (HAL). *Genomics* **1995**, *29*, 98−104.

(3) Schwede, T. F.; Rétey, J.; Schulz, G. E. Crystal Structure of Histidine Ammonia-Lyase Revealing a Novel Polypeptide Modification as the Catalytic Electrophile. *Biochemistry* **1999**, *38*, 5355−5361.

(4) Christianson, C. V.; Montavon, T. J.; Van Lanen, S. G.; Shen, B.; Bruner, S. D. The Structure of L-Tyrosine 2,3-Aminomutase from the C-1027 Enediyne Antitumor Antibiotic Biosynthetic Pathway. *Biochemistry* **2007**, *46*, 7205−7214.

(5) Kyndt, J. A.; Meyer, T. E.; Cusanovich, M. A.; Van Beeumen, J. J. Characterization of a Bacterial Tyrosine Ammonia Lyase, a Biosynthetic Enzyme for the Photoactive Yellow Protein. *FEBS Lett.* **2002**, *512*, 240−244.

(6) Vogt, T. Phenylpropanoid Biosynthesis. *Mol. Plant* **2010**, *3*, 2−20.

(7) Poppe, L.; Paizs, C.; Kovács, K.; Irimie, F.-D.; Vértessy, B. Preparation of Unnatural Amino Acids with Ammonia-Lyases and 2,3-Aminomutases. In *Unnatural Amino Acids. Methods in Molecular Biology (Methods and Protocols)*; Pollegioni, L., Servi, S., Ed.; Humana Press; New York, USA, 2012; pp 3−19.

(8) Wang, L.; Gamez, A.; Sarkissian, C. N.; Straub, M.; Patch, M. G.; Han, G. W.; Striepeke, S.; Fitzpatrick, P.; Scriver, C. R.; Stevens, R. C. Structure-Based Chemical Modification Strategy for Enzyme Replacement Treatment of Phenylketonuria. *Mol. Genet. Metab.* **2005**, *86*, 134−140.

(9) FDA. *FDA Approves a New Treatment for PKU, a Rare and Serious Genetic Disease*. Press Announcements, 2018.

(10) Hermes, J. D.; Weiss, P. M.; Cleland, W. W. Use of Nitrogen-15 and Deuterium Isotope Effects to Determine the Chemical Mechanism of Phenylalanine Ammonia-Lyase. *Biochemistry* **1985**, *24*, 2959−2967.

(11) Schuster, B.; Retey, J. The Mechanism of Action of Phenylalanine Ammonia-Lyase: The Role of Prosthetic Dehydroalanine. *Proc. Natl. Acad. Sci. U.S.A.* **1995**, *92*, 8433−8437.

(12) Poppe, L.; Rétey, J. Friedel-Crafts-Type Mechanism for the Enzymatic Elimination of Ammonia from Histidine and Phenylalanine. *Angew. Chem., Int. Ed.* **2005**, *44*, 3668−3688.

(13) Pilbák, S.; Farkas, Ö.; Poppe, L. Mechanism of the Tyrosine Ammonia Lyase Reaction-Tandem Nucleophilic and Electrophilic Enhancement by a Proton Transfer. *Chem.—Eur. J.* **2012**, *18*, 7793−7802.

(14) Mutatu, W.; Klettke, K. L.; Foster, C.; Walker, K. D. Unusual Mechanism for an Aminomutase Rearrangement: Retention of Configuration at the Migration Termini. *Biochemistry* **2007**, *46*, 9785−9794.

(15) Ratnayake, N. D.; Wanninayake, U.; Geiger, J. H.; Walker, K. D. Stereochemistry and Mechanism of a Microbial Phenylalanine Aminomutase. *J. Am. Chem. Soc.* **2011**, *133*, 8531−8533.

(16) Krug, D.; Müller, R. Discovery of Additional Members of the Tyrosine Aminomutase Enzyme Family and the Mutational Analysis of CmdF. *ChemBioChem* **2009**, *10*, 741−750.
(17) Chesters, C.; Wilding, M.; Goodall, M.; Micklefield, J. Thermal Bifunctionality of Bacterial Phenylalanine Aminomutase and Ammonia Lyase Enzymes. *Angew. Chem., Int. Ed.* **2012**, *51*, 4344−4348.
(18) Heberling, M. M.; Masman, M. F.; Bartsch, S.; Wybenga, G. G.; Dijkstra, B. W.; Marrink, S. J.; Janssen, D. B. Ironing out Their Differences: Dissecting the Structural Determinants of a Phenylalanine Aminomutase and Ammonia Lyase. *ACS Chem. Biol.* **2015**, *10*, 989−997.
(19) Baedeker, M.; Schulz, G. E. Structures of Two Histidine Ammonia-Lyase Modifications and Implications for the Catalytic Mechanism. *Eur. J. Biochem.* **2002**, *269*, 1790−1797.
(20) Calabrese, J. C.; Jordan, D. B.; Boodhoo, A.; Sariaslani, S.; Vannelli, T. Crystal Structure of Phenylalanine Ammonia Lyase: Multiple Helix Dipoles Implicated in Catalysis. *Biochemistry* **2004**, *43*, 11403−11416.
(21) Ritter, H.; Schulz, G. E. Structural Basis for the Entrance into the Phenylpropanoid Metabolism Catalyzed by Phenylalanine Ammonia-Lyase. *Plant Cell* **2004**, *16*, 3426−3436.
(22) Louie, G. V.; Bowman, M. E.; Moffitt, M. C.; Baiga, T. J.; Moore, B. S.; Noel, J. P. Structural Determinants and Modulation of Substrate Specificity in Phenylalanine-Tyrosine Ammonia-Lyases. *Chem. Biol.* **2006**, *13*, 1327−1338.
(23) Moffitt, M. C.; Louie, G. V.; Bowman, M. E.; Pence, J.; Noel, J. P.; Moore, B. S. Discovery of Two Cyanobacterial Phenylalanine Ammonia Lyases: Kinetic and Structural Characterization. *Biochemistry* **2007**, *46*, 1004−1012.
(24) Montavon, T. J.; Christianson, C. V.; Festin, G. M.; Shen, B.; Bruner, S. D. Design and Characterization of Mechanism-Based Inhibitors for the Tyrosine Aminomutase SgTAM. *Bioorg. Med. Chem. Lett.* **2008**, *18*, 3099−3102.
(25) Wang, L.; Gamez, A.; Archer, H.; Abola, E. E.; Sarkissian, C. N.; Fitzpatrick, P.; Wendt, D.; Zhang, Y.; Vellard, M.; Bliesath, J.; Bell, S. M.; Lemontt, J. F.; Scriver, C. R.; Stevens, R. C. Structural and Biochemical Characterization of the Therapeutic Anabaena variabilis Phenylalanine Ammonia Lyase. *J. Mol. Biol.* **2008**, *380*, 623−635.
(26) Cooke, H. A.; Bruner, S. D. Probing the Active Site of MIO-Dependent Aminomutases, Key Catalysts in the Biosynthesis of *β*-Amino Acids Incorporated in Secondary Metabolites. *Biopolymers* **2010**, *93*, 802−810.
(27) Feng, L.; Wanninayake, U.; Strom, S.; Geiger, J.; Walker, K. D. Mechanistic, Mutational, and Structural Evaluation of aTaxusPhenylalanine Aminomutase. *Biochemistry* **2011**, *50*, 2919−2930.
(28) Wu, B.; Szymański, W.; Wybenga, G. G.; Heberling, M. M.; Bartsch, S.; de Wildeman, S.; Poelarends, G. J.; Feringa, B. L.; Dijkstra, B. W.; Janssen, D. B. Mechanism-Inspired Engineering of Phenylalanine Aminomutase for Enhanced *β*-Regioselective Asymmetric Amination of Cinnamates. *Angew. Chem., Int. Ed.* **2012**, *51*, 482−486.
(29) Strom, S.; Wanninayake, U.; Ratnayake, N. D.; Walker, K. D.; Geiger, J. H. Insights into the Mechanistic Pathway of thePantoea agglomeransPhenylalanine Aminomutase. *Angew. Chem., Int. Ed.* **2012**, *51*, 2898−2902.
(30) Wybenga, G. G.; Szymanski, W.; Wu, B.; Feringa, B. L.; Janssen, D. B.; Dijkstra, B. W. Structural Investigations into the Stereochemistry and Activity of a Phenylalanine-2,3-Aminomutase from Taxus chinensis. *Biochemistry* **2014**, *53*, 3187−3198.
(31) Weise, N. J.; Ahmed, S. T.; Parmeggiani, F.; Galman, J. L.; Dunstan, M. S.; Charnock, S. J.; Leys, D.; Turner, N. J. Zymophore Identification Enables the Discovery of Novel Phenylalanine Ammonia Lyase Enzymes. *Sci. Rep.* **2017**, *7*, 13691.
(32) Jun, S.-Y.; Sattler, S. A.; Cortez, G. S.; Vermerris, W.; Sattler, S. E.; Kang, C. Biochemical and Structural Analysis of Substrate Specificity of a Phenylalanine Ammonia-Lyase. *Plant Physiol.* **2018**, *176*, 1452−1468.
(33) Nagy, E. Z. A.; Tork, S. D.; Lang, P. A.; Filip, A.; Irimie, F. D.; Poppe, L.; Toşa, M. I.; Schofield, C. J.; Brem, J.; Paizs, C.; Bencze, L. C. Mapping the Hydrophobic Substrate Binding Site of Phenylalanine Ammonia-Lyase from Petroselinum crispum. *ACS Catal.* **2019**, *9*, 8825−8834.
(34) Pilbák, S.; Tomin, A.; Rétey, J.; Poppe, L. The Essential Tyrosine-Containing Loop Conformation and the Role of the C-Terminal Multi-Helix Region in Eukaryotic Phenylalanine Ammonia-Lyases. *FEBS J.* **2006**, *273*, 1004−1019.
(35) Bartsch, S.; Wybenga, G. G.; Jansen, M.; Heberling, M. M.; Wu, B.; Dijkstra, B. W.; Janssen, D. B. Redesign of a Phenylalanine Aminomutase into a Phenylalanine Ammonia Lyase. *ChemCatChem* **2013**, *5*, 1797−1802.
(36) Attanayake, G.; Walter, T.; Walker, K. D. Understanding Which Residues of the Active Site and Loop Structure of a Tyrosine Aminomutase Define Its Mutase and Lyase Activities. *Biochemistry* **2018**, *57*, 3503−3514.
(37) Bata, Z.; Qian, R.; Roller, A.; Horak, J.; Bencze, L. C.; Paizs, C.; Hammerschmidt, F.; Vértessy, B. G.; Poppe, L. A Methylidene Group in the Phosphonic Acid Analogue of Phenylalanine Reverses the Enantiopreference of Binding to Phenylalanine Ammonia-Lyases. *Adv. Synth. Catal.* **2017**, *359*, 2109−2120.
(38) Appert, C.; Logemann, E.; Hahlbrock, K.; Schmid, J.; Amrhein, N. Structural and Catalytic Properties of the Four Phenylalanine Ammonia-Lyase Isoenzymes from Parsley (Petroselinum crispum Nym.). *Eur. J. Biochem.* **1994**, *225*, 491−499.
(39) Lüdemann, S. K.; Lounnas, V.; Wade, R. C. How Do Substrates Enter and Products Exit the Buried Active Site of Cytochrome P450cam? 1. Random Expulsion Molecular Dynamics Investigation of Ligand Access Channels and Mechanisms. *J. Mol. Biol.* **2000**, *303*, 813−830.
(40) Peräkylä, M. Ligand Unbinding Pathways from the Vitamin D Receptor Studied by Molecular Dynamics Simulations. *Eur. Biophys. J.* **2009**, *38*, 185−198.
(41) Lopata, A.; Leveles, I.; Bendes, Á. Á.; Viskolcz, B.; Vértessy, B. G.; Jójárt, B.; Tóth, J. A Hidden Active Site in the Potential Drug Target Mycobacterium tuberculosis DUTPase Is Accessible through Small Amplitude Protein Conformational Changes. *J. Biol. Chem.* **2016**, *291*, 26320−26331.
(42) Urban, P.; Lautier, T.; Pompon, D.; Truan, G. Ligand Access Channels in Cytochrome P450 Enzymes: A Review. *Int. J. Mol. Sci.* **2018**, *19*, 1617.
(43) Kokkonen, P.; Bednar, D.; Pinto, G.; Prokop, Z.; Damborsky, J. Engineering Enzyme Access Tunnels. *Biotechnol. Adv.* **2019**, *37*, 107386.
(44) Pravda, L.; Sehnal, D.; Toušek, D.; Navrátilová, V.; Bazgier, V.; Berka, K.; Svobodová Vařeková, R.; Koča, J.; Otyepka, M. MOLEonline: A Web-Based Tool for Analyzing Channels, Tunnels and Pores (2018 Update). *Nucleic Acids Res.* **2018**, *46*, W368−W373.
(45) Stourac, J.; Vavra, O.; Kokkonen, P.; Filipovic, J.; Pinto, G.; Brezovsky, J.; Damborsky, J.; Bednar, D. Caver Web 1.0: Identification of Tunnels and Channels in Proteins and Analysis of Ligand Transport. *Nucleic Acids Res.* **2019**, *47*, W414−W422.
(46) Varga, A.; Bata, Z.; Csuka, P.; Bordea, D. M.; Vértessy, B. G.; Marcovici, A.; Irimie, F. D.; Poppe, L.; Bencze, L. C. A Novel Phenylalanine Ammonia-Lyase from Kangiella koreensis. *Stud. Univ. Babes-Bolyai, Chem.* **2017**, *62*, 293−308.
(47) Csuka, P.; Juhász, V.; Kohári, S.; Filip, A.; Varga, A.; Sátorhelyi, P.; Bencze, L. C.; Barton, H.; Paizs, C.; Poppe, L. Pseudomonas fluorescensStrain R124 Encodes Three Different MIO Enzymes. *ChemBioChem* **2018**, *19*, 411−418.
(48) Chen, C. S.; Fujimoto, Y.; Girdaukas, G.; Sih, C. J. Quantitative Analyses of Biochemical Kinetic Resolutions of Enantiomers. *J. Am. Chem. Soc.* **1982**, *104*, 7294−7299.
(49) Langer, M.; Pauling, A.; Rétey, J. The Role of Dehydroalanine in Catalysis by Histidine Ammonia Lyase. *Angew. Chem., Int. Ed.* **1995**, *34*, 1464−1465.

https://doi.org/10.1021/acscatal.1c00266
ACS Catal. XXXX, XXX, XXX−XXX

(50) Bartsch, S.; Bornscheuer, U. T. A Single Residue Influences the Reaction Mechanism of Ammonia Lyases and Mutases. *Angew. Chem., Int. Ed.* **2009**, *48*, 3362−3365.
(51) Weiser, D.; Bencze, L. C.; Bánóczi, G.; Ender, F.; Kiss, R.; Kókai, E.; Szilágyi, A.; Vértessy, B. G.; Farkas, Ö.; Paizs, C.; Poppe, L. Phenylalanine Ammonia-Lyase-Catalyzed Deamination of an Acyclic Amino Acid: Enzyme Mechanistic Studies Aided by a Novel Microreactor Filled with Magnetic Nanoparticles. *ChemBioChem* **2015**, *16*, 2283−2288.
(52) Bencze, L. C.; Filip, A.; Bánóczi, G.; Toşa, M. I.; Irimie, F. D.; Gellért, Á.; Poppe, L.; Paizs, C. Expanding the substrate scope of phenylalanine ammonia-lyase from Petroselinum crispum towards styrylalanines. *Org. Biomol. Chem.* **2017**, *15*, 3717−3727.
(53) Gloge, A.; Langer, B.; Poppe, L.; Rétey, J. The Behavior of Substrate Analogues and Secondary Deuterium Isotope Effects in the Phenylalanine Ammonia-Lyase Reaction. *Arch. Biochem. Biophys.* **1998**, *359*, 1−7.
(54) Rice, F. O.; Teller, E. The Role of Free Radicals in Elementary Organic Reactions. *J. Chem. Phys.* **1938**, *6*, 489−496. Rice, F. O.; Teller, E. Corrections to Paper "The Role of Free Radicals in Elementary Organic Reactions". *J. Chem. Phys.* **1939**, *7*, 199.
(55) Hine, J. The Principle of Least Motion. Application to Reactions of Resonance-Stabilized Species. *J. Org. Chem.* **1966**, *31*, 1236−1244.
(56) Sinnott, M. L. The Principle of Least Nuclear Motion and the Theory of Stereoelectronic Control. *Adv. Phys. Org. Chem.* **1988**, *24*, 113−204.
(57) Schütz, A.; Golbik, R.; König, S.; Hübner, G.; Tittmann, K. Intermediates and Transition States in Thiamin Diphosphate-Dependent Decarboxylases. A Kinetic and NMR Study on Wild-Type Indolepyruvate Decarboxylase and Variants Using Indolepyruvate, Benzoylformate, and Pyruvate as Substrates. *Biochemistry* **2005**, *44*, 6164−6179.
(58) Weise, N. J.; Parmeggiani, F.; Ahmed, S. T.; Turner, N. J. The Bacterial Ammonia Lyase EncP: A Tunable Biocatalyst for the Synthesis of Unnatural Amino Acids. *J. Am. Chem. Soc.* **2015**, *137*, 12977−12983.
(59) Zhu, L.; Yang, J.; Feng, G.; Ge, F.; Li, W.; Song, P.; Tao, Y.; Zhou, Z. Investigation into Isomerization Reaction of Phenylalanine Aminomutase from Pantoea agglomerans. *Enzyme Microb. Technol.* **2020**, *132*, 109428.
(60) Zhu, L.; Ge, F.; Li, W.; Song, P.; Tang, H.; Tao, Y.; Liu, Y.; Du, G. One Step Synthesis of Unnatural *β*-Arylalanines Using Mutant Phenylalanine Aminomutase from Taxus chinensis with High *β*-Regioselectivity. *Enzyme Microb. Technol.* **2018**, *114*, 22−28.
(61) Hodgins, D. S. Yeast Phenylalanine Ammonia-Lyase. Purification, Properties, and the Identification of Catalytically Essential Dehydroalanine. *J. Biol. Chem.* **1971**, *246*, 2977−2985.
(62) Brezovsky, J.; Babkova, P.; Degtjarik, O.; Fortova, A.; Gora, A.; Iermak, I.; Rezacova, P.; Dvorak, P.; Smatanova, I. K.; Prokop, Z.; Chaloupkova, R.; Damborsky, J. Engineering a de Novo Transport Tunnel. *ACS Catal.* **2016**, *6*, 7597−7610.
(63) Kabsch, W. Xds. *Acta Crystallogr., Sect. D: Biol. Crystallogr.* **2010**, *66*, 125−132.
(64) McCoy, A. J.; Grosse-Kunstleve, R. W.; Adams, P. D.; Winn, M. D.; Storoni, L. C.; Read, R. J. Phasercrystallographic software. *J. Appl. Crystallogr.* **2007**, *40*, 658−674.
(65) Adams, P. D.; Afonine, P. V.; Bunkóczi, G.; Chen, V. B.; Davis, I. W.; Echols, N.; Headd, J. J.; Hung, L.-W.; Kapral, G. J.; Grosse-Kunstleve, R. W.; McCoy, A. J.; Moriarty, N. W.; Oeffner, R.; Read, R. J.; Richardson, D. C.; Richardson, J. S.; Terwilliger, T. C.; Zwart, P. H. PHENIX: A Comprehensive Python-Based System for Macromolecular Structure Solution. *Acta Crystallogr., Sect. D: Biol. Crystallogr.* **2010**, *66*, 213−221.
(66) Emsley, P.; Lohkamp, B.; Scott, W. G.; Cowtan, K. Features and Development of Coot. *Acta Crystallogr., Sect. D: Biol. Crystallogr.* **2010**, *66*, 486−501.
(67) Humphrey, W.; Dalke, A.; Schulten, K. VMD: Visual Molecular Dynamics. *J. Mol. Graphics* **1996**, *14*, 33−38.
(68) R Core Team. *R: A Language and Environment for Statistical Computing*; R Foundation for Statistical Computing, 2016.

https://doi.org/10.1021/acscatal.1c00266
ACS Catal. XXXX, XXX, XXX−XXX